Available online at www.sciencedirect.com
SCIENCE DIRECT®
Journal of the European Ceramic Society 25 (2005) 649–654
www.elsevier.com/locate/jeurceramsoc

Analysis of the nanoindentation load–displacement curves measured on high-purity fine-grained alumina

Jianghong Gong*, Zhijian Peng, Hezhuo Miao

Department of Materials Science and Engineering, Tsinghua University, Beijing 100084, PR China

Received 12 February 2004; accepted 10 April 2004

Available online 15 June 2004

Abstract

This paper conducted a preliminary examination on the effect of microstructural inhomogeneity on the reproducibility of the nanoindentation data. Nanoindentation tests were conducted on a high-purity, fine-grained alumina ceramic. It was found that the reproducibility of the nanoindentation data were somewhat poor. The nanoindentation data were then analyzed with the widely employed Oliver–Pharr method to yield the hardness, *H*, and the Young's modulus, *E*. Large scatters were observed in the resultant *H* and *E*. These experimental findings revealed that microstructural inhomogeneity may play an important role in the material response to nanoindentation.

Keywords: Hardness; Mechanical properties; Nanoindentation; Al_2O_3

1. Introduction

Nanoindentation test has been established as an important tool for the mechanical characterization of materials on the submicron scale. Such a test is usually conducted using instrumented machines with which indenter load, *P*, and indenter displacement, *h*, can be continuously and simultaneously recorded during indenter loading and unloading. The unloading data are then analyzed to yield the hardness, *H*, and the Young's modulus, *E*.

Although nanoindentation test has been widely employed during the past decades to measure the mechanical properties for numerous materials including polycrystalline ceramics,[1–5] little attention has been paid to the effect of microstructural inhomogeneity on the reproducibility of the nanoindentation data. In fact, when being examined at the submicron scale, any polycrystalline ceramic should be considered to be inhomogeneous. Thus, one can expect that, when being indented at different positions, or to different depth at the same position, of the specimen surface, the response of the test material to nanoindentation may be different due mainly to the fact that the indentation-induced deformation (and fracture) is dominated mainly by the local, rather than the bulk, mechanical properties. As a result, the nanoindentation load–displacement curves obtained from different loading–unloading cycles would be different with each other and such a difference may be very significant in some cases.

The present study was designed to conduct a preliminary examination on the effect of microstructural inhomogeneity on the reproducibility of the nanoindentation data. A high-purity, fine-grained alumina ceramic was selected as the examined material because this material has an average grain size of about 0.9 μm, which is comparable to the indenter penetration depth during nanoindentation and, as a result, such a small grain size would make it much easier to examine the effect of microstructural inhomogeneity.

2. Experimental

A high-purity, fine-grained alumina ceramic was selected as the test material for the present study. According to the information provided by the supplier, this polycrystalline alumina was prepared from alumina powder mixed with small amount of oxide additives by cold isostatically pressing, pressureless sintering at 1250 °C for 90 min, and then hot-isostatically pressing (HIP) at 1350 °C and 140 MPa for 45 min. The density of the test specimen was measured us-

* Corresponding author. Fax: +86 10 62771160.
E-mail address: gong@mail.tsinghua.edu.cn (J. Gong).

0955-2219/$ – see front matter © 2004 Elsevier Ltd. All rights reserved.
doi:10.1016/j.jeurceramsoc.2004.04.003

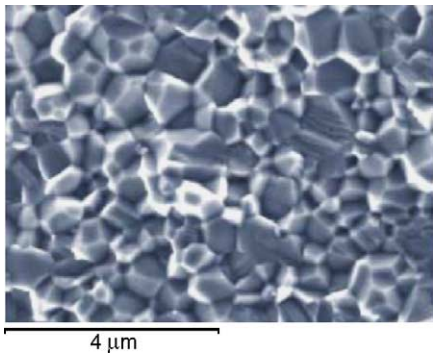

Fig. 1. SEM micrograph showing the fracture surface of the test specimen.

ing Archimedes' principle to be 3.98 g/cm^3, about 99.9% of the theoretical value. Fig. 1 shows the SEM micrograph of a typical microstructure of the fracture surface of the test specimen. Clearly, the material exhibits a much small and fairly uniform grain structure. No evident pore can be found in the fracture surface. The average grain size of the test material was estimated to be 0.9 μm.

The specimen used for nanoindentation test was cut directly from the as-HIPed plates, mounted in bakelite, ground flat using a diamond grinding wheel, and then polished carefully with successively finer diamond paste to yield a scratch-free, mirror-like surface finish suitable for indentation.

Nanoindentation experiments were carried out using a fully calibrated Nano Indenter XP (Nanoinstruments Innovation Center, MTS Systems, TN, USA) equipped with a standard Berkovich indenter. Experiments were conducted using a load–time sequence like that shown in Fig. 2. For each loading–unloading cycle, loading and unloading lasted 15 s, respectively, and a dwell time of 30 s at each peak load was used. During each test run, a personal computer collected and stored data for the load and displacement as the indenter was driven into the sample (loading segment) and then withdrawn from it (unloading segment). The raw data were then used to construct the load–displacement plot. A total of 10 indentations were made at random-selected, different positions on the specimen surface, correspondingly, 10 load–displacement curves, each containing seven loading–unloading cycles, were obtained.

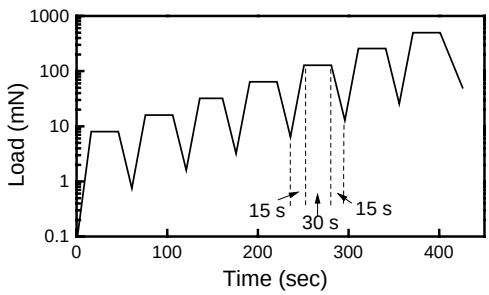

Fig. 2. The load–time sequence used in the nanoindentation experimental procedure.

3. Results and discussion

3.1. Analysis of the loading curves

Fig. 3 shows some of the load–displacement (P–h) curves obtained in the present study. Table 1 summarizes the minimum, maximum, mean value and the standard deviation of the 10 data of the penetration depth, h_{max}, measured at each peak load, P_{max}. Clearly, both Fig. 3 and Table 1 indicate that the reproducibility of the P–h curve is somewhat poor. Note that these P–h curves were obtained by indenting at the different positions of the specimen surface, respectively, and the average penetration depth at the maximum peak load level, $P_{max} = 505$ mN, is only 1158.4 nm, being comparable to the average grain size of the test material, about 900 nm. There seems to be reason to believe that the poor reproducibility of the measured P–h curve may be attributed to differences between the local microstructural features in the vicinity of each indentation position. In other words, the experimental facts shown in Fig. 3 and Table 1 seem to indicate that the measured P–h curve may depend strongly on the local microstructural features and, as a result, the mechanical properties deduced from the analysis of the P–h curve are only the local, rather than the bulk, properties of the test material.

A very interesting feature of the data shown in Table 1 is that the coefficient of variation of h_{max} exhibits a decreasing tendency with increasing peak load. This seems to be an indirect support for the above analysis. As the peak load increases, the indenter penetration depth increases and the indentation zone of influence expands. As a result, the indentation zone of influence would "feel" more microstructural features and the effect of microstructural inhomogeneity would weaken.

Although it is very difficult to examine the exact details of the microstructural features in the vicinity of the indentation site, some useful information may be obtained by comparing the P–h curves measured at different positions in the specimen surface.

Censored views of some of the measured P–h curves are shown in Fig. 4 to give a comparison between the material

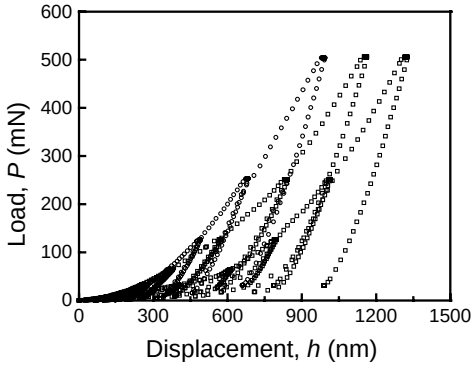

Fig. 3. Representative load–displacement curves obtained in the present study.

Table 1
Statistical properties of the penetration depth, h_{max}, measured at different peak load level

P_{max} (mN)	7.9	15.9	31.7	63.5	126.5	251.9	505.1
h_{max} (nm)							
Minimum	93.5	146.9	224.4	338.5	490.6	682.7	992.3
Maximum	217.9	376.0	474.1	620.5	796.4	1014.7	1338.1
Mean	144.2	227.4	321.2	446.0	600.9	824.5	1158.4
σ[a]	42.6	76.6	84.4	103.9	106.3	103.7	116.9
C_v[a]	0.295	0.337	0.263	0.233	0.177	0.126	0.101

[a] σ and C_v denote the standard deviation and the coefficient of variation of the measured h_{max}, respectively.

responses at different positions of the surface to indentation during the first two loading–unloading cycles. Fig. 4(a) indicates that, when being indented, the position B deforms much easier than the position A. Among all the 10 indentation experiments, indentation made at the position A yields the minimum penetration depth, $h_{max} = 93.5$ nm, at the peak load of 7.9 mN. Therefore, it is reasonable to infer that the position A is located nearly in the center of a grain and the polished surface of this grain is one of the harder crystallographic planes. Indenter penetration at the position B, $h_{max} = 117.3$ nm for $P_{max} = 7.9$ mN, is somewhat larger than that at the position A and one can infer that the position B may be located within a grain whose polished surface is one of the softer crystallographic planes.

Fig. 4(b) shows another two censored P–h curves measured at the positions C and D, respectively. The shape of the P–h curve for the position C is similar to those for the positions A and B. The former differs from the latter only in the penetration depth. Therefore, the microstructural features in the vicinity of the position C may be similar to that of the position B.

The shape of the P–h curve for the position D is rather different from those shown in Fig. 4(a). At first, the indenter penetration depth increases gradually with increasing indenter load and the data points fall along the P–h curve for the position C. However, when the load increases above about 5 mN, the data points begin to departure from the curve C and, at the same load, a larger penetration depth was observed for the position D when compared with the position C. This seems to indicate that the indenter encounters a soft microstructural feature whose elastic/plastic properties are rather different from those of the alumina grain. Thus, one can infer that the position D may be located at, at least very near to, a grain boundary or a pore. The relatively lower hardness of the grain boundary or the pore makes the indentation on the position D yield the maximum penetration depth, $h_{max} = 217.9$ nm, at the peak load of $P_{max} = 7.9$ mN.

Near-surface boundaries or pores may also affect the shape of the P–h curve in the high load region. A typical example is shown in Fig. 5. During the indentation at the position E, a sharp increase in the indenter penetration depth, from about 1000 to 1170 nm, was observed when the indenter load increased to about 340 mN. This seems to indicate

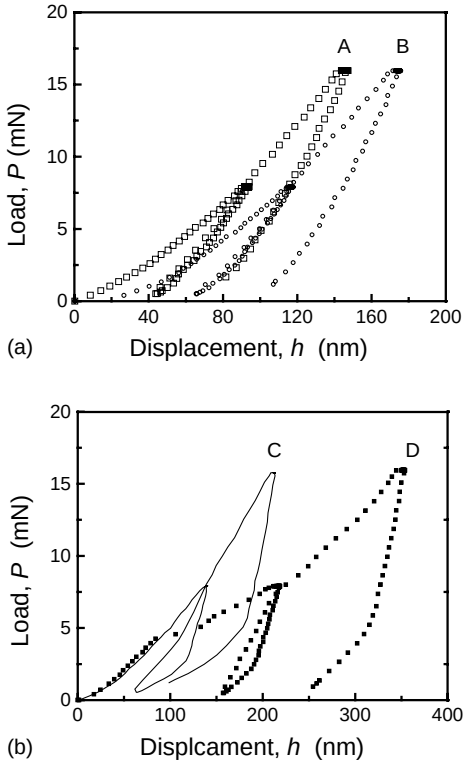

Fig. 4. Censored views of some of the measured P–h curves showing the first two loading–unloading cycles.

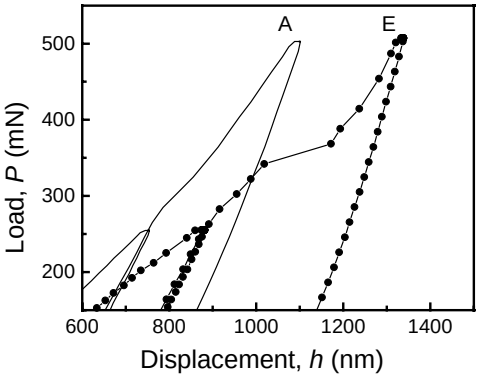

Fig. 5. Expanded views of the P–h curves measured at the positions A and E.

that the indenter encounters, or acrosses, a grain boundary whose zone of influence is about 170 nm in thickness.

3.2. Description of the unloading curves

The effect of microstructural inhomogeneity on the reproducibility of the load–displacement curve may also be examined from the quantitative analyses of the unloading data. In the most commonly employed Oliver–Pharr method for analyzing the nanoindentation data, an empirical power law is selected to describe the unloading data[1]

$$P = \alpha(h - h_f)^m \tag{1}$$

where α and m are empirically determined fitting parameters and h_f is the final displacement after complete unloading and also determined by curve fitting.

It should be pointed out that a basis assumption for using Eq. (1) to describe the nanoindentation unloading behavior is[1] that the unloading is pure elastic, i.e., the unloading curve and the corresponding reloading curve should overlap with each other. In most of the loading–unloading–reloading cycles examined in the present study, the resultant unloading and reloading curves are nearly the same; see for example Figs. 4(a) and 5. As typically shown in Fig. 4(b), however, distinct hysteresis loops were observed in some unloading–reloading cycles in this study, indicating there is an evident reverse plasticity upon unloading. In the following text, analyses and discussion will be conducted with the unloading curves associated with a nearly pure elastic unloading procedure.

The load–displacement data for each unloading curve except those associated with evident reserve plasticity were analyzed according to Eq. (1) and the results are summarized in Table 2. As can be seen, both α and m exhibit large scatters. Such large scatters may be attributed to the effect of microstructural inhomogeneity. Pharr and Bolshakov[6] proposed an "effective indenter" model to explain the physical meaning of Eq. (1). In this model, the Berkovich indenter is modeled as an "effective indenter" whose geometry is determined by the shape of the plastic hardness impression formed during indentation and both the power law exponent m and the power law coefficient α are predicted to be functions of the Young's modulus and the hardness of the test material.[6] Based on the "effective indenter" model, the large scatters in the experimentally determined m and α seem to indicate that the hardness and the Young's modulus of the material in the vicinity of the indentation site may be different in different loading–unloading cycles. Thus, one can conclude that the microstructural inhomogeneity may play an important role in the material response to nanoindentation.

3.3. Hardness and Young's modulus

In the nanoindentation experiments, the hardness and the Young's modulus are usually derived from[1]

$$H = \frac{P_{max}}{A} \tag{2}$$

and

$$S = \left(\frac{dP}{dh}\right)_{h=h_{max}} = \gamma\left(\frac{2}{\sqrt{\pi}}\right)E_r\sqrt{A} \tag{3}$$

where A is the projected contact area; S, unloading stiffness measured at the maximum penetration depth, h_{max}; γ, a correction factor due to the lack of axial symmetry[7] and the reduced modulus E_r is defined as

$$\frac{1}{E_r} = \frac{1-\nu^2}{E} + \frac{1-\nu_I^2}{E_I} \tag{4}$$

where E and ν are the Young's modulus and the Poisson's ratio of the test material, and E_I and ν_I are the Young's modulus and the Poisson's ratio of the indenter.

The projected contact area, A, included in Eqs. (2) and (3) is a function of the contact depth, h_c, which is given by[1]

$$h_c = h_{max} - \varepsilon\left(\frac{P_{max}}{S}\right) \tag{5}$$

where ε is a constant. In general, the Berkovich indenter is modeled as a paraboloid punch (i.e., $m = 1.5$ in Eq. (1)). Consequently, the value of ε is 0.75.

For a perfect Berkovich indenter, we have $A = 24.5h_c^2$. However, a real indenter is never perfect due to some tip rounding. To take account of the effect of the indenter-tip-rounding on the determination of the projected contact area, the following area function for the Berkovich

Table 2
Summary of the best-fit values of parameters included in Eq. (1) for describing the unloading curves observed in nanoindentation experiments

Peak load P_{max} (mN)	$\alpha \times 10^2$ (mN/nm^m)			m		
	Minimum	Maximum	Mean	Minimum	Maximum	Mean
7.9	1.29	2.17	1.58 ± 0.40	1.45	1.62	1.54 ± 0.07
15.9	0.56	2.65	1.74 ± 0.79	1.45	1.85	1.60 ± 0.15
31.7	1.32	5.03	3.05 ± 1.34	1.40	1.72	1.51 ± 0.12
63.5	1.78	6.33	4.14 ± 1.43	1.39	1.66	1.51 ± 0.08
126.5	0.77	6.46	4.77 ± 2.59	1.41	1.82	1.54 ± 0.16
251.9	2.68	12.00	6.13 ± 2.92	1.38	1.62	1.49 ± 0.07
505.1	1.06	11.53	4.65 ± 3.30	1.42	1.79	1.59 ± 0.13

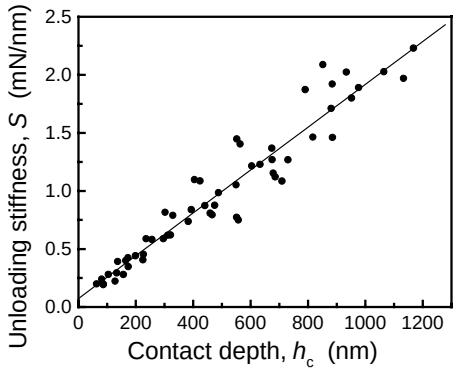

Fig. 6. Relationship between h_c and S.

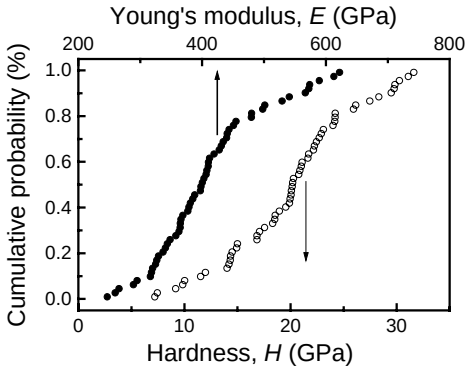

Fig. 7. Cumulative distribution functions of the hardness, H, and the Young's modulus, E.

indenter with a rounding tip was selected for the present study[8,9]

$$A = 24.5(h_c + h_d)^2 \quad (6)$$

where h_d is the effective truncation length of the indenter tip.

Substituting Eq. (6) into Eq. (3) yields

$$S = \frac{2}{\sqrt{\pi}} E_r \sqrt{24.5}(h_c + h_d) \quad (7)$$

Eq. (7) predicts that a linear relationship exists between S and h_c if E_r can be treated as a constant.

Using the best-fit values of α and m, the initial unloading slope, S, and the contact depth, h_c, were calculated with Eqs. (3) and (5), respectively, for each measured unloading curve except those associated with evident reserve plasticity. Then the resultant S and h_c were analyzed according to Eq. (7) and the results are shown in Fig. 6. It can be seen that all the data points fall around the best-fit line. The discrepancies between the experimental data and the best-fit line are somewhat large and this can be understood by noting the fact that the reduced modulus E_r is not a constant. From the slope and the intercept of the best-fit line shown in Fig. 6, the effective truncation length of the indenter tip, h_d, is estimated to be 39.5 nm. Nanoindentation experiments were also conducted on soda-lime glass with the same indenter and analysis of the experimental data yielded an h_d-value of 37.5 nm.[10] The good agreement between these two data implies that Eq. (7) may provide an approximate description for the experimental data obtained in the present study.

The hardness, H, and the Young's modulus, E, were determined from each measured unloading curve except those associated with evident reserve plasticity according to the method outlined above and the results are now shown in Fig. 7. As can be seen, the scatters in the resultant H and E are significantly large: H varies from 7.2 to 31.6 GPa and E from 246.9 to 622.0 GPa. The large scatters imply that the hardness and the Young's modulus determined from the individual unloading curve are only the measures of the local, rather than the bulk, properties of the test material. Furthermore, these results support the discussion made in the preceding subsection and demonstrate that the local mechanical properties indeed vary significantly with the indentation position.

Statistical analysis of the experimental data shown in Fig. 7 yields that H has an average value of 20.0 GPa and a standard deviation of 6.0 GPa, while E has an average value of 409 GPa and a standard deviation of 90 GPa. These data warrant further comment. The microhardness of the high-purity, fine-grained alumina examined here was determined to be 17.8 ± 0.4 GPa corresponding to an indentation load of 10 N. On the other hand, the Young's modulus for polycrystalline alumina was generally reported to be about 390 GPa.[11] Note that there may exist an indentation size effect in the hardness, i.e., the measured hardness usually decreases with the increasing test load.[12,13] Compared with these typical data, the average values of H and E obtained in the present study seem to be reasonable estimations for the bulk properties of the test material. This seems not to be surprising because the averaging of a large number of test results is equivalent to applying the rule of mixture, the empirical approach for predicting the property of a composite. The individual experimental result is only a measure of the local property and, from the viewpoint of statistics, one can expect that, if the number of the data points is not sufficiently large, the average value would differ significantly from the bulk value measured with conventional methods.

Fig. 8 shows the ratio of h_f/h_c, a measure of the elastic recovery during unloading, as a function of the local me-

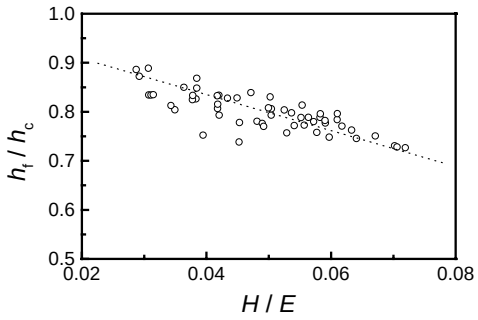

Fig. 8. h_f/h_c-ratio as a function of the local mechanical properties H/E.

chanical properties, H/E, and a strong correlation between these two quantities is evident. Theoretical analysis[14,15] revealed that h_f/h_c is a decreasing function of the mechanical properties H/E. The experimental result shown in Fig. 8 is consistent with the theoretical prediction and, thus, suggests that it is the local, rather than the bulk, properties that dominate the material response to nanoindentation.

4. Concluding remarks

Nanoindentation experiments were conducted on a high-purity, fine-grained alumina ceramic. It was found that the reproducibility of the load–displacement curve is somewhat poor. Closely examining the shape of the measured load–displacement curves revealed that the microstructural inhomogeneity may play an important role in the material response to nanoindentation. The hardness and the Young's modulus deduced from the analysis of the unloading curves also exhibited large scatter and should be treated as the local, rather than the bulk mechanical properties of the test material.

Although the present study is only preliminary work and only one polycrystalline ceramic was examined, there is reason to believe that similar phenomenon may also be observed when conducting the nanoindentation experiments on materials whose microstructural features have a characteristic dimension comparable to or smaller than the characteristic dimension of the examined indenter penetration depth. Therefore, it seems to be unreliable to measure the hardness and Young's modulus by conducting a small quantity of nanoindentation tests, especially in the case that the reproducibility of the measured load–displacement curve is somewhat poor.

Acknowledgements

The authors would like to thank Dr. Wenjie Si of Tsinghua University, China, for providing the alumina sample employed in this study. The authors would also like to thank Mrs. Yang Gao for her assistance in conducting the nanoindentation experiments.

References

1. Oliver, W. C. and Pharr, G. M., An improved technique for determining hardness and elastic modulus using load and displacement sensing indentation experiments. *J. Mater. Res.* 1992, **7**, 1564–1583.
2. Nix, W. D., Elastic and plastic properties of thin films on substrates: nanoindentation techniques. *Mater. Sci. Eng. A* 1997, **234–236**, 37–44.
3. Krell, A. and Schädlich, S., Nanoindentation hardness of submicrometer alumina ceramics. *Mater. Sci. Eng. A* 2001, **307**, 172–181.
4. Ullner, C., Beckmann, J. and Morrell, R., Instrumented indentation test for advanced technical ceramics. *J. Eur. Ceram. Soc.* 2002, **22**, 1183–1189.
5. Fischer-Cripps, A. C., Analysis of instrumented indentation test data for functionally graded materials. *Surf. Coat. Technol.* 2003, **168**, 136–141.
6. Pharr, G. M. and Bolshakov, A., Understanding nanoindentation unloading curves. *J. Mater. Res.* 2002, **17**, 2660–2671.
7. Hay, J. C., Bolshakov, A. and Pharr, G. M., A critical examination of the fundamental relations used in the analysis of nanoindentation data. *J. Mater. Res.* 1999, **14**, 2296–2305.
8. Malzbender, J., With, G. D. and Toonder, J. D., The P–h^2 relationship in indentation. *J. Mater. Res.* 2000, **15**, 1209–1212.
9. Sawa, T. and Tanaka, K., Simplified method for analyzing nanoindentation data and evaluating performance of nanoindentation instruments. *J. Mater. Res.* 2001, **16**, 3084–3096.
10. Gong, J. H., Miao, H. Z. and Peng, Z. J., Analysis of the nanoindentation data measured with a Berkovich indenter for brittle materials: effect of the residual contact stress. *Acta Mater.* 2004, **52**, 785–793.
11. Franco, A., Roberts, S. G. and Warren, P. D., Fracture toughness. *Acta Mater.* 1997, **45**, 1009–1015.
12. Quinn, G. D. and Quinn, J. B., Indentation brittleness of ceramics: a fresh approach. *J. Mater. Sci.* 1997, **32**, 4331–4346.
13. Gong, J. H., Wu, J. J. and Guan, Z. D., Examination of the indentation size effect in low-load Vickers hardness testing of ceramics. *J. Eur. Ceram. Soc.* 1999, **19**, 2625–2631.
14. Lawn, B. R. and Howes, V. R., Elastic recovery at hardness indentations. *J. Mater. Sci.* 1981, **16**, 2745–2752.
15. Cheng, Y. T., Li, Z. and Cheng, C. M., Scaling relationships for indentation measurements. *Philos. Mag.* 2002, **82**, 1821–1829.